Hindawi Publishing Corporation
Shock and Vibration
Volume 2016, Article ID 8021690, 15 pages
http://dx.doi.org/10.1155/2016/8021690

Research Article

Control Performance and Robustness of Pounding Tuned Mass Damper for Vibration Reduction in SDOF Structure

Qichao Xue,[1,2] Jingcai Zhang,[1] Jian He,[1] and Chunwei Zhang[2,3]

[1]*College of Aerospace and Civil Engineering, Harbin Engineering University, Harbin, China*
[2]*School of Civil Engineering, Qingdao University of Technology, Qingdao, China*
[3]*Institute for Infrastructure Engineering, Western Sydney University, Sydney, NSW, Australia*

Correspondence should be addressed to Chunwei Zhang; chunwei.zhang@westernsydney.edu.au

Received 31 August 2016; Accepted 27 October 2016

Academic Editor: Ganging Song

This paper investigates the control performance of pounding tuned mass damper (PTMD) in reducing the dynamic responses of SDOF (Single Degree of Freedom) structure. Taking an offshore jacket-type platform as an example, the optimal damping ratio and the gap between mass block and viscoelastic material are presented depending on a parametric study. Control efficiency influenced by material properties and contact geometries for PTMD is analyzed here, as well as robustness of the device. The results of numerical simulations indicated that satisfactory vibration mitigation and robustness can be achieved by an optimally designed PTMD. Comparisons between PTMD and traditional TMD demonstrate the advantages of PTMD, not only in vibration suppression and costs but also in effective frequency bandwidth.

1. Introduction

An offshore platform is essential equipment for ocean oil development with high construction cost, and it may lead to serious damage when subjected to seismic effects [1, 2]. Therefore, an effective vibration reduction solution is necessary for offshore platforms. Tuned mass damper (TMD) is a traditional control device installed on the offshore platform to reduce the seismic vibration responses. Kawano et al. [3] first investigated seismic responses of the offshore platform with TMD and indicated that TMD can reduce seismic vibration effectively. Since then, many researches have focused on TMD applications on platforms. For instance, Wu et al.'s study [4] on high response performance of TMD indicates that TMD can significantly reduce the vibration of the platform and a remarkable decreased power spectral density can be achieved.

However, TMDs have several disadvantages in utilizing structure vibration control. First of all, most of TMD devices need to be tuned to the first natural frequency of the primary structure to obtain better control performance. Once the excitation's frequency deviates from the first natural frequency, TMD's vibration reduction will decrease sharply and even cause terrible adverse effects. At this time, although an extra damper attaching to TMD can suppress the adverse effects, it is costly and will lead to waste of space due to the large motion of the mass block.

In order to avoid the foregoing disadvantages and achieve satisfactory vibration control performance, many new analysis technologies have been applied to improve TMD. Almazan et al. [5] proposed a bidirectional and homogeneous tuned mass damper (BH-TMD) for passive control of vibrations. Both experimental and numerical simulation results demonstrate the superiority of the modified TMD system over the traditional one. A conceptual system for a semiactive tuned mass damper (STMD) with variable damping coefficients and stiffness values was presented by Chey et al. [6]. Sun and Nagarajaiah [7] presented a new algorithm for STMD to adjust the damping coefficient for different excitation. Jafarabad et al. [8] installed a hybrid damping system to control the seismic vibration which contains a friction damper device (FDD) and a tuned mass damper (TMD). Mohebbi et al. [9] analyzed optimum parameters of multiple tuned mass dampers (MTMDs) for different design criteria under seismic excitation.

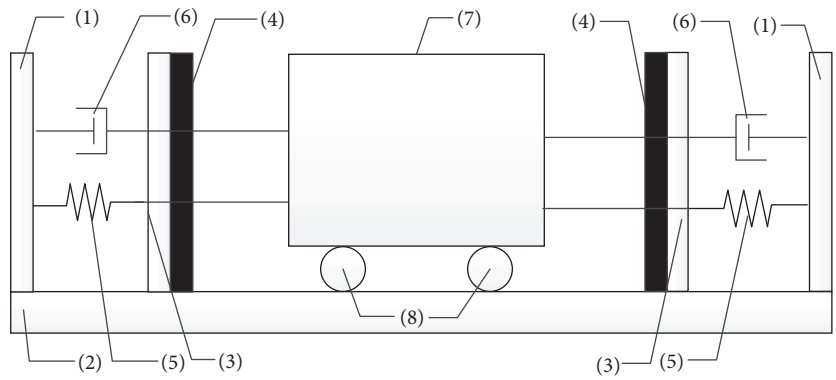

(1) Limiter of TMD
(2) Bottom board
(3) Limiter of pounding device
(4) Viscoelastic material
(5) Spring
(6) Damper
(7) Mass block
(8) Rolling bearings

Figure 1: Schematic graph of PTMD with viscoelastic material layers.

Despite the former new analysis technologies, some novel control devices were proposed on platforms too. Huo and Li [10] developed a circular tuned liquid column damper (CTLCD) to control the platform's torsional responses under seismic loads. Li et al.'s [11] research shows that satisfactory vibration mitigation can be achieved by a new shape memory alloy (SMA) damper. Ou et al. [12] proposed a damping isolation system which was composed of rubber bearings and viscous dampers for controlling vibration. Komachi et al. [13] applied a friction damper device to a steel jacket platform located in an active zone and investigated the performance when subjected to seismic excitation. Mousavi et al. [14, 15] employed a tuned liquid column-gas damper (TLCGD) to suppress the seismic vibration and obtained optimum geometric parameters for a platform. Sarrafan et al. [16] presented an intelligent nonlinear neurofuzzy control strategy for magnetorheological (MR) damper system in order to adjust controlling force for different excitations. Lotfollahi-Yaghin et al. [17] verified the seismic control performance of tuned liquid damper (TLD) on typical offshore jacket-type platforms excited by El Centro, Kobe, and Tabas earthquakes.

Pounding tuned mass damper (PTMD) is proposed as a combination of traditional TMD and pounding effects by Zhang et al. [18]. Zhang et al. [18–22] investigated the vibration control performance of PTMD on power transmission tower and subsea jumpers, as well as traffic signal poles. There is rarely a result showing the performance of PTMD on offshore platform.

In this paper, taking an offshore jacket platform as an example, control performance and robustness of PTMD for vibration reduction in SDOF structure are analyzed to investigate the seismic control performance. Influences of different parameters are discussed, including damping ratio, gap between mass block and viscoelastic layer, contact geometries, robustness, and viscoelastic properties. Furthermore, a comparison between PTMD and traditional TMD is presented to verify the advantages of PTMD.

Table 1: Parameters of the offshore jacket platform.

	Test 1	Test 2		
Real platform	f/Hz		ξ_1/%	m_1/t
	0.90	0.85	4.0–5.5	3127
Simplified model	f/Hz	k_1/kN·s^{-1}	c_1/kN·(m·s^{-1})	m_1/kg
	0.87	93436	1367	3127000

2. Schematic of PTMD with Viscoelastic layers

As an improvement of TMD, PTMD consists of two parts: a traditional TMD and a limiter layered by viscoelastic materials. Gaps between mass block and viscoelastic material are reserved as shown in Figure 1. When the relative motion occurs between mass block and viscoelastic layer without pounding effect, PTMD acts as a TMD. Otherwise, the mass block will impact the viscoelastic layer, which will produce pounding force as an extra controlling effect, and energy will be dissipated during the pounding process. One of the most remarkable advantages of this device is that controlling forces come from not only resonant force but also pounding force during the impact.

3. Modeling

3.1. Modeling of the System. As a widely used platform type in the Bohai Sea of China, JZ20-2MUQ offshore jacket platform plays an important role in the field of petroleum recovery. The platform consists of three parts: 3-story frame for living, 2-story frame for working, and the jackets. Ou et al.'s research [23] shows that the platform can be simplified to a Single Degree of Freedom (SDOF) structure since the mass of the upper quarter is dominant to the whole structure. Figure 2 shows the JZ20-2MUQ offshore jacket platform and the simplified model. The basic parameters are given in Table 1 based on Ou et al.'s research.

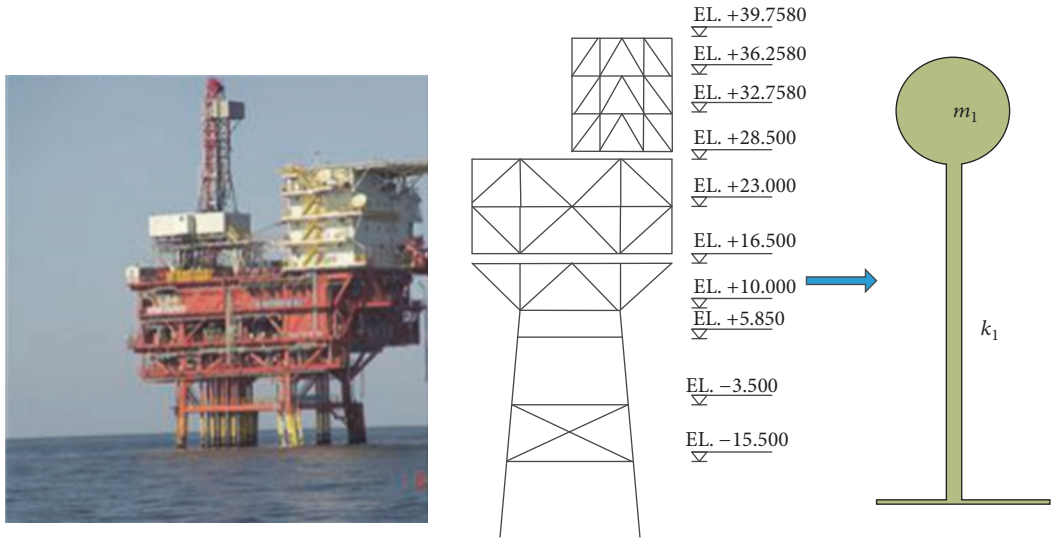

(a) A real platform (b) The elevation (c) The simplified model

Figure 2: JZ20-2MUQ offshore jacket platform.

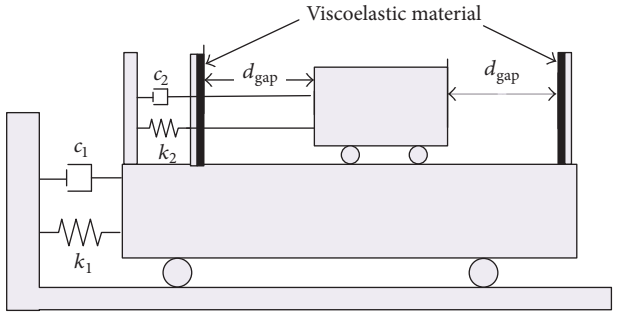

Figure 3: Schematic of a SDOF structure controlled by PTMD.

3.2. Dynamic Equations of the System. The schematic of a SDOF structure controlled by PTMD is illustrated in Figure 3, and the motion equation of the system can be expressed as

$$\begin{bmatrix} m_1 & 0 \\ 0 & m_2 \end{bmatrix} \cdot \begin{Bmatrix} \ddot{x}_1 \\ \ddot{x}_2 \end{Bmatrix} + \begin{bmatrix} c_1 + c_2 & -c_2 \\ -c_2 & c_2 \end{bmatrix} \cdot \begin{Bmatrix} \dot{x}_1 \\ \dot{x}_2 \end{Bmatrix} + \begin{bmatrix} k_1 + k_2 & -k_2 \\ -k_2 & k_2 \end{bmatrix} \cdot \begin{Bmatrix} x_1 \\ x_2 \end{Bmatrix} = \begin{Bmatrix} P \sin \omega t + H(d) F \\ -H(d) F \end{Bmatrix}, \tag{1}$$

where m_1 and m_2 are mass of primary structure and PTMD, respectively. $\ddot{x}_1$, $\dot{x}_1$, and x_1 are acceleration, velocity, and displacement of the primary structure. $\ddot{x}_2$, $\dot{x}_2$, and x_2 are acceleration, velocity, and displacement of the PTMD. c_1 and c_2 are stiffness of primary structure and PTMD, respectively. k_1 and k_2 are stiffness of primary structure and PTMD, respectively. F is the pounding force induced by collisions between mass block and viscoelastic layer. $H(d)$ is Havsid function

$$H(d) = \begin{cases} 1 & |d| - d_{gap} > 0 \\ 0 & \text{otherwise,} \end{cases} \tag{2}$$

where d represents the relative displacement between the PTMD and the primary structure and is calculated by (3). d_{gap} is the gap between the mass block and the viscoelastic layer. Hence,

$$d = x_2 - x_1, \tag{3}$$

where P is the amplitude of the external force; in order to simplify the calculation process, $P = 1$.

3.3. Modeling of Pounding Force

3.3.1. Pounding Force Expressions for Two Kinds of Contact Geometries. Figure 4(a) is a sketch for a mass block with sphere head pounding to a plane surface, which will be utilized later in this paper to simulate vibration performance of PTMD. Figure 4(b) shows that an end plane of the column is pounding to plane, which will be calculated as a comparison to discuss influences of contact geometries. The pounding force can be calculated by (4) according to contact mechanics [24]:

$$\begin{aligned} F_c &= \frac{4}{3} R_1^{1/2} E^* \delta_1^{3/2} \quad \text{for sphere to plane,} \\ F_c &= 2 R_1 E^* \delta_1 \quad \text{for column to plane,} \end{aligned} \tag{4}$$

where R_1 is the radius of the hemisphere or ending round plane for column. $R = 0.5$ meters in this paper. δ_1 is

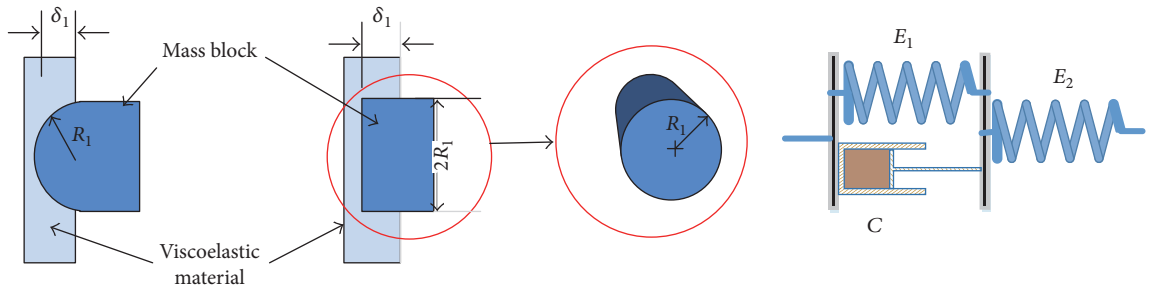

(a) Sphere to plane (b) Column to plane (c) 3-parameter model

Figure 4: Schematic of contact geometries and 3-parameter viscoelastic model.

the penetration displacement. E^* is the equivalent elasticity modulus and can be derived by the following expression:

$$\frac{1}{E^*} = \frac{\left(1-\vartheta_s^2\right)}{E_s} + \frac{\left(1-\vartheta_p^2\right)}{E_p}, \tag{5}$$

where υ_p, υ_s, E_p, and E_s are Poisson's ratio and modulus of elasticity for polymer and steel, respectively. In case of polymer contact with steel, the modulus of elasticity for steel is far larger than polymer, and the expression of E^* can be simplified as follows:

$$E^* = \frac{E_p}{1-\vartheta_p^2}. \tag{6}$$

According to the Correspondence Principle of viscoelasticity, pounding force expressions can be deduced by inverse Laplace transformation from (4) and (6):

$$F_{(t)} = \frac{4}{3}\frac{R_1^{1/2}}{1-\vartheta_p^2}\ell^{-1}\left(\frac{\overline{Q}(s)}{\overline{P}(s)}\right)\delta_1^{3/2}(t) \quad \text{for sphere to plane,}$$
$$F_{(t)} = 2\frac{R_1}{1-\vartheta_p^2}\ell^{-1}\left(\frac{\overline{Q}(s)}{\overline{P}(s)}\right)\delta_1(t) \quad \text{for column to plane.} \tag{7}$$

For linear viscoelastic materials, $\overline{Q}(s)$ and $\overline{P}(s)$ are polynomial of parameter s and they can be calculated automatically as a transfer function with different initial values by MATLAB/Simulink.

4. Parametric Study

To obtain optimal parametric settings of PTMD, damping ratio of the PTMD, gap between mass block and viscoelastic layer, contact geometries, and viscoelastic properties are discussed in this section. Unless otherwise indicated, constitutive parameters of viscoelastic material in this paper are shown in Table 2. And E_1, E_2, and C_1 are the spring parameters and dash-pot parameter for 3-parameter model of viscoelastic material in Figure 4(c).

Table 2: Constitutive parameters of the viscoelastic material.

E_1/Pa	E_2/Pa	C/kN·(m·s^{-1})	E^*/Pa
2.041*E*5	2.041*E*5	3.9*E*4	1.08*E*5

For comparison, performance of an optimal TMD is presented based on Ioi and Ikeda's research [25], in which optimal frequency and damping ratio can be expressed as

$$f_{\text{opt}} = \frac{1}{1+\mu} - \left(0.241 + 1.7\mu - 2.6\mu^2\right)\xi_s^2, \tag{8}$$

$$\xi_{\text{opt}} = \sqrt{\frac{3\mu}{8(1+\mu)}} + \left(0.13 + 0.12\mu + 0.4\mu^2\right)\xi_2 - \left(0.01 + 0.09\mu + 3\mu^2\right)\xi_2, \tag{9}$$

where f_{opt} and ξ_{opt} are the optimal frequency and damping ratio for the TMD, μ is mass ratio, and ξ_s is damping ratio of primary structure.

4.1. Damping Ratio. In order to illustrate the parameters' influence more accurately and efficiently, the dimensionless method is applied to the data analysis:

$$\delta = \frac{d_{\text{gap}}}{\delta_s}, \quad \delta_s = \frac{P}{k_1}, \quad f_e = \frac{\omega}{\omega_1}, \tag{10}$$

where d_{gap} is the gap between mass block and viscoelastic material. δ is the dimensionless gap, and δ_s is the static displacement of the primary structure. P is the amplitude of the sinusoidal wave which is input into the SDOF system, and k_1 is the structural stiffness of the primary structure. The frequency ratio which is defined as f_e is an index of degree for sinusoidal wave deviating from the natural frequency, and ω and ω_1 represent the sinusoidal wave frequency and natural frequency of the primary structure, respectively.

Dynamic amplification factor, defined as R in (11), is introduced to evaluate the performance of controlling devices.

In addition, the mass ratio is assumed to be 2.0% which is the most common selection in engineering practice. Hence,

$$R = \frac{x_{1,\text{peak}}}{\delta_s}, \tag{11}$$

where $x_{1,\text{peak}}$ is the peak value of the displacement in steady state subjected to sinusoidal wave excitation. The dimensionless displacement and acceleration of the primary structure, named X and A, respectively, can be calculated as follows:

$$\begin{aligned} X &= \frac{x}{\delta_s}, \\ A &= \ddot{X}, \end{aligned} \tag{12}$$

where x is the displacement of the primary structure during the excitation and A is the second derivative in time of X.

Damping ratio of PTMD, defined as ξ_2, can be calculated as

$$\xi_2 = \frac{c_2}{2\mu m_1 \omega_2}, \tag{13}$$

where c_2 and ω_2 are damping coefficient and circular frequency of PTMD, m_1 is the mass of the platform, and μ is the mass ratio. Thus, we can conclude that only in case of $\xi_2 = 0$ is PTMD undamped.

Figure 5 illustrates the relationship between R and f_e with different damping ratios in the relative frequency domain. It can be observed from Figure 5(a) that an undamped PTMD has obvious magnification in structure responses. For instance, maximum value of R is 28.3 for PTMD when δ is equal to 2, and it is almost triple those controlled by TMD. In this situation, PTMD is not suitable as a vibration control device.

A damper in vibration control device can effectively eliminate magnification effect ($\xi_2 \neq 0$). Figure 5(c) displays the performance of PTMD with different gaps when an optimal damper parameter is applied. Although vibration control performance for PTMD is much better than TMD when f_e varies from 0.9 to 1.3, there is a significantly inverse effect on primary structure response for PTMD in case f_e is less than 0.9. That means the optimal damping ratio which is based on TMD is no longer applicable to PTMD due to pounding effects.

From Figures 5(b)–5(e), R diminishes with the increasing of damping ratio from 0 to $3.0\xi_{\text{opt}}$ when the gap value is a constant. As ξ_2 is $3.0\xi_{\text{opt}}$, PTMD shows a more remarkable performance compared to TMD. Moreover, R rises with the increase of gap in this situation which indicates that impact played a positive role in vibration reduction.

However, Figure 5(f) shows that the structures vibrate more severely in case of $\xi_2 = 4.0\xi_{\text{opt}}$ than those with the same gap and $\xi_2 = 3.0\xi_{\text{opt}}$. Further, PTMD shows a poorer performance than TMD when δ is equal to 10. In this situation, although an additional damper may enhance the efficiency of PTMD, an excessive damping ratio may lead to an opposite effect.

From Figures 5(a)–5(f), we can obtain an optimal damping ratio for the best performance of PTMD in this case: $\xi_{2,\text{opt}} = 3.0\xi_{\text{opt}}$.

4.2. Influences of Gap. From an energy viewpoint, energy can be dissipated from the damper in TMD or PTMD, as well as the impact process between mass block and viscoelastic material. A small gap in PTMD means that the mass will impact the viscoelastic material more severely and frequently. In an extreme case where the gap is large enough, the impact will not happen and PTMD turns into a traditional TMD.

Figure 5 clearly revealed that a sufficient gap is indispensable to an undamped PTMD to avoid the adverse effect caused by the impact. To quantify the energy dissipation of PTMD, the root mean square (RMS) of displacement and the acceleration of the primary structure are defined as in (14). A smaller RMS means more energy will be dissipated or transformed to dampers. Hence,

$$\begin{aligned} \text{RMS}_{X_1} &= \sqrt{\frac{\sum_1^n (X_{1i})^2}{n}}, \\ X_i &= \frac{P x_i}{k_1}. \end{aligned} \tag{14}$$

Figure 6 plots the changing trend of RMS_{A_1} and RMS_{X_1} along with dimensionless gap. In this case, $\xi_2 = 3\xi_t$ with mass ratio 2%, and n is the number of values in the time history record.

It can be observed from Figure 6 that both of RMS_A and RMS_X decrease with the increasing of δ and finally tend to be a constant under a low frequency of sinusoidal wave excitation (where f_e is 0.7 and 0.8). Considering that PTMD will degenerate to TMD when RMS turns to a constant, impact has a negative effect on PTMD's performance in this situation. That means a large gap is required for low frequency excitation.

However, for relatively high frequency excitation with f_e higher than 0.9, both RMS_A and RMS_X increase with the rising of the dimensionless gap. An optimal gap value will avoid the negative effect and maximize the positive effect. This is always needed for PTMD due to the randomness and variety of earthquakes. From Figure 6, the optional dimensionless gap δ is about 2 for offshore jacket platform in this paper.

4.3. Material Properties. Properties of the viscoelastic material layer in PTMD will give different vibration reduction results. It is clear that the material with a higher E^* can induce a larger pounding force under the same situation, which may enhance the controlling force and get more momentum exchanged during an impact. Two additional materials, named type A and B (shown in Table 3), together with former materials in Table 2, are utilized to investigate the influence of material properties on PTMD. The results are illustrated in Figure 7.

Figure 7(b) shows time history of the dimensionless displacement of the platform controlled by PTMD with different materials in case of $f_e = 1.1$. It can be seen in this case that a higher equivalent elastic modulus can improve the controlling performance. However, in Figure 7(a) which corresponds to the case $f_e = 0.85$, it is indicated that the equivalent elasticity modulus has an opposite effect which

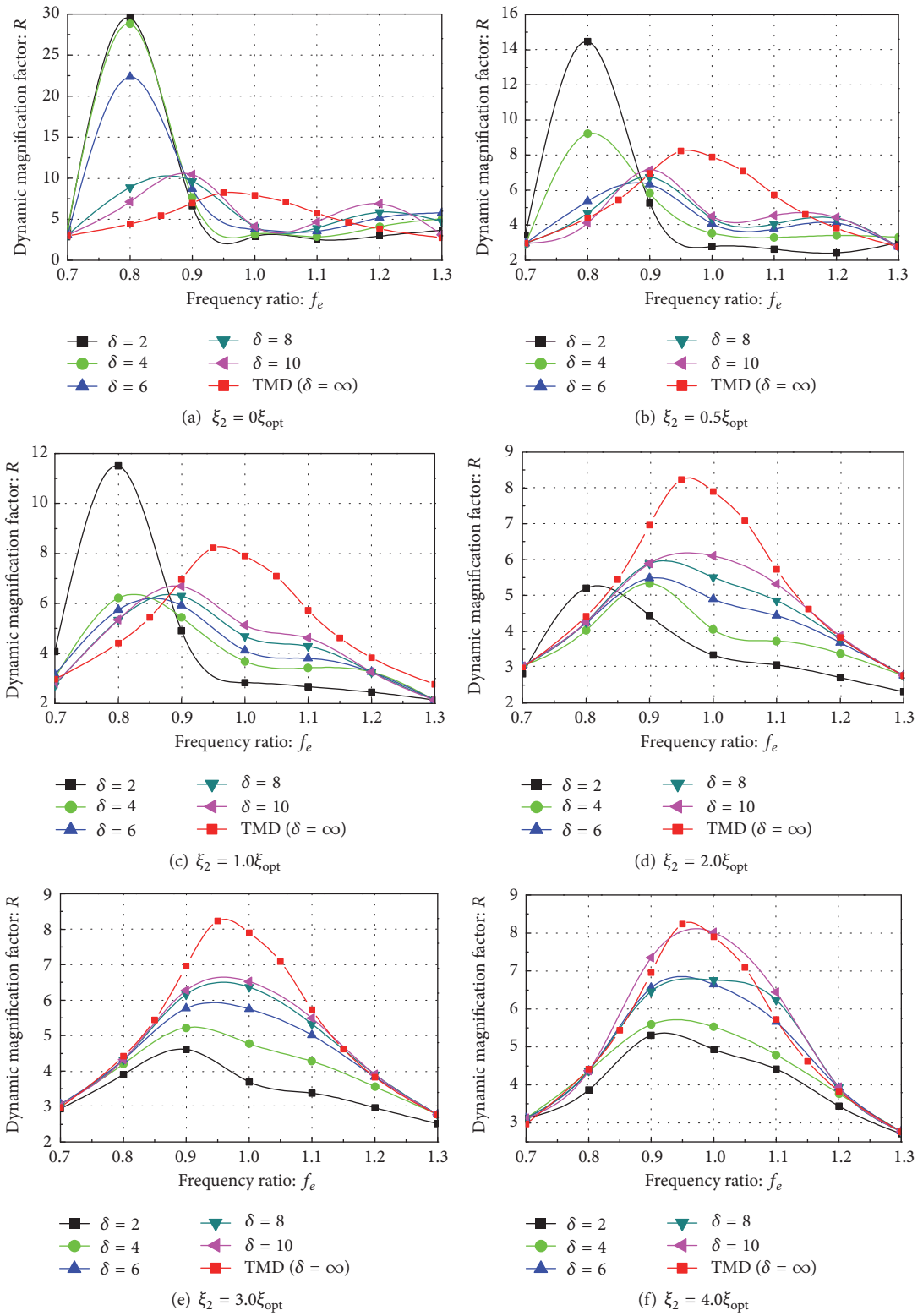

FIGURE 5: Responses of the controlled structure with different damping ratios.

leads to a poorer control result. Comparing Figures 7(a) and 7(b), we can conclude that a material with high equivalent elasticity modulus can enhance the efficiency when the excitation's frequency is higher than the natural frequency of primary structure. Otherwise, it will weaken the vibration reduction.

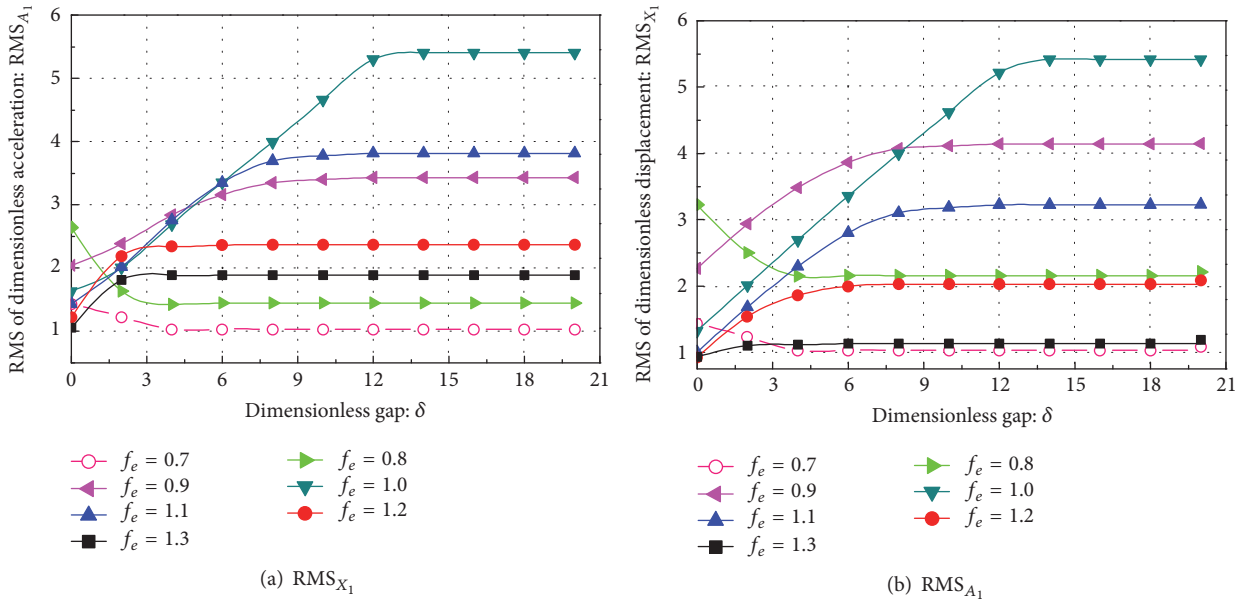

(a) RMS$_{X_1}$ (b) RMS$_{A_1}$

Figure 6: Primary structure RMS curve along with the change of δ ($\xi_2 = 3\xi_{opt}$, $\mu = 2\%$).

Table 3: Parameters of the additional materials.

Type ID	E_1/Pa	E_2/Pa	C/kN·(m·s^{-1})	E^*/Pa
A	2.041*E*6	2.041*E*6	3.9*E*5	1.08*E*6
B	2.041*E*7	2.041*E*7	3.9*E*6	1.08*E*7

4.4. Contact Geometries. As an indispensable part of controlling force for PTMD, pounding force is determined not only by material properties but also by the geometry of colliding bodies. Figure 8 illustrates the responses of the platform controlled by PTMD with two types of contact geometries, which were shown in Figures 4(a) and 4(b). For materials calculated in this paper, a better performance can be achieved by a sphere head than by a plane one. But differences of reduction between the two types of contact geometries are no more than 7% for both peak value and RMS. For type A material which is presented in Table 3, there is almost no difference between the two kinds of geometries. It can be concluded that geometric properties of the contact have a little effect on the performance of PTMD.

5. Robustness of PTMD

Tuning to the natural frequency of primary structure is the most important purpose for traditional TMD design. However, it is difficult to measure the natural frequency of the structure accurately. The primary structure natural frequency for the platform is not a constant due to the operating environment loads, such as depth of water and equipment replacement, which will lead to robustness of PTMD. Influences of tuned sinusoidal vibration, detuning vibration, and free vibration will be investigated here to study the robustness of PTMD.

To quantify the degree of deviation between an optimal frequency and tuned frequency in TMD and PTMD, the detuning ratio (DTR) is defined as follows:

$$\mathrm{DTR} = \frac{f_{\mathrm{damper}} - f_{\mathrm{opt}}}{f_{\mathrm{opt}}} \cdot 100\%, \tag{15}$$

where f_{damper} is the frequency of PTMD or TMD and f_{opt} is the optimal frequency which was expressed by (8).

5.1. Tuned Excitation Vibration. The value of frequency 0.74 Hz corresponds to −15% of the detuning ratio and 1.00 Hz corresponds to 15%. Dimensionless displacement X_1 in steady state can reach as large as 32.8 for the structure without control. However, for an installed PTMD, the maximum X_1 can be limited below 2.5 and 3.4 which correspond to 0.74 Hz and 1.00 Hz. In other words, X_1 can be sharply reduced by 89.6% and 74.9%, respectively.

The simulation results in Figure 9(a) illustrate that PTMD is effective even without tuning, which proves its good performance with robustness. Responses with the same detuning ratio TMD are presented in Figure 9(b), and the maximum value of X_1 can be reduced to 15.4 and 12.7, which correspond to reductions of 53.0% and 61.3% separately. This verifies that PTMD has superior performance over the traditional TMD in this case.

5.2. Free Vibration. Figure 10 shows free vibration responses of the primary structure when dimensionless initial displacement X_1 is equal to 40. It shows that displacement responses are damped rapidly for both frequencies 0.74 Hz and 1.00 Hz with PTMD control in Figure 10(a). The peak value of X_1 reduces by 80% in 22.4 s if a 1.00 Hz PTMD is installed. And when it comes to 0.74 Hz, the duration time will drop to 15 s.

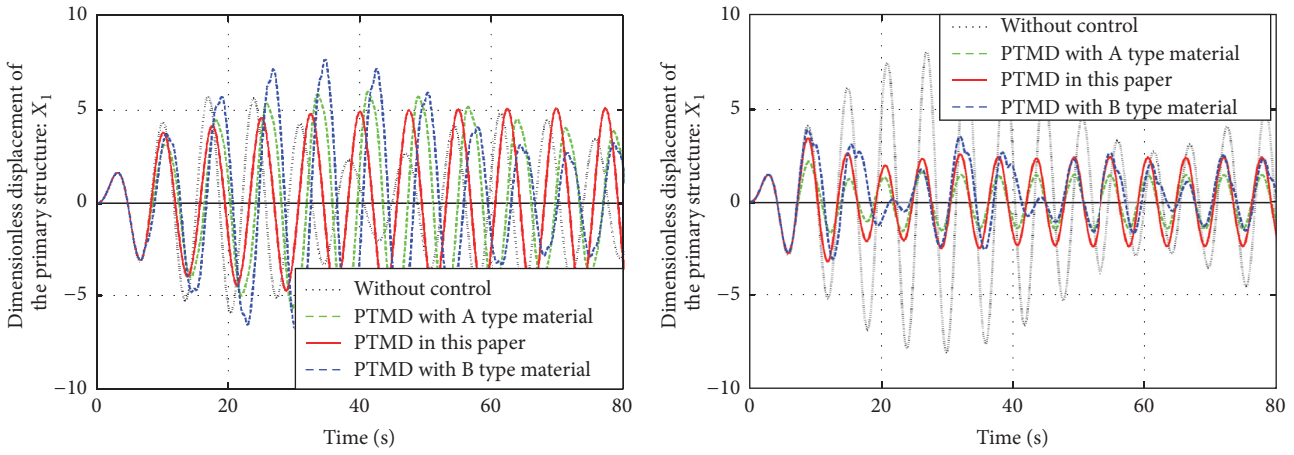

(a) $f_e = 0.85$ (b) $f_e = 1.1$

Figure 7: Control performance of PTMD with different types of materials.

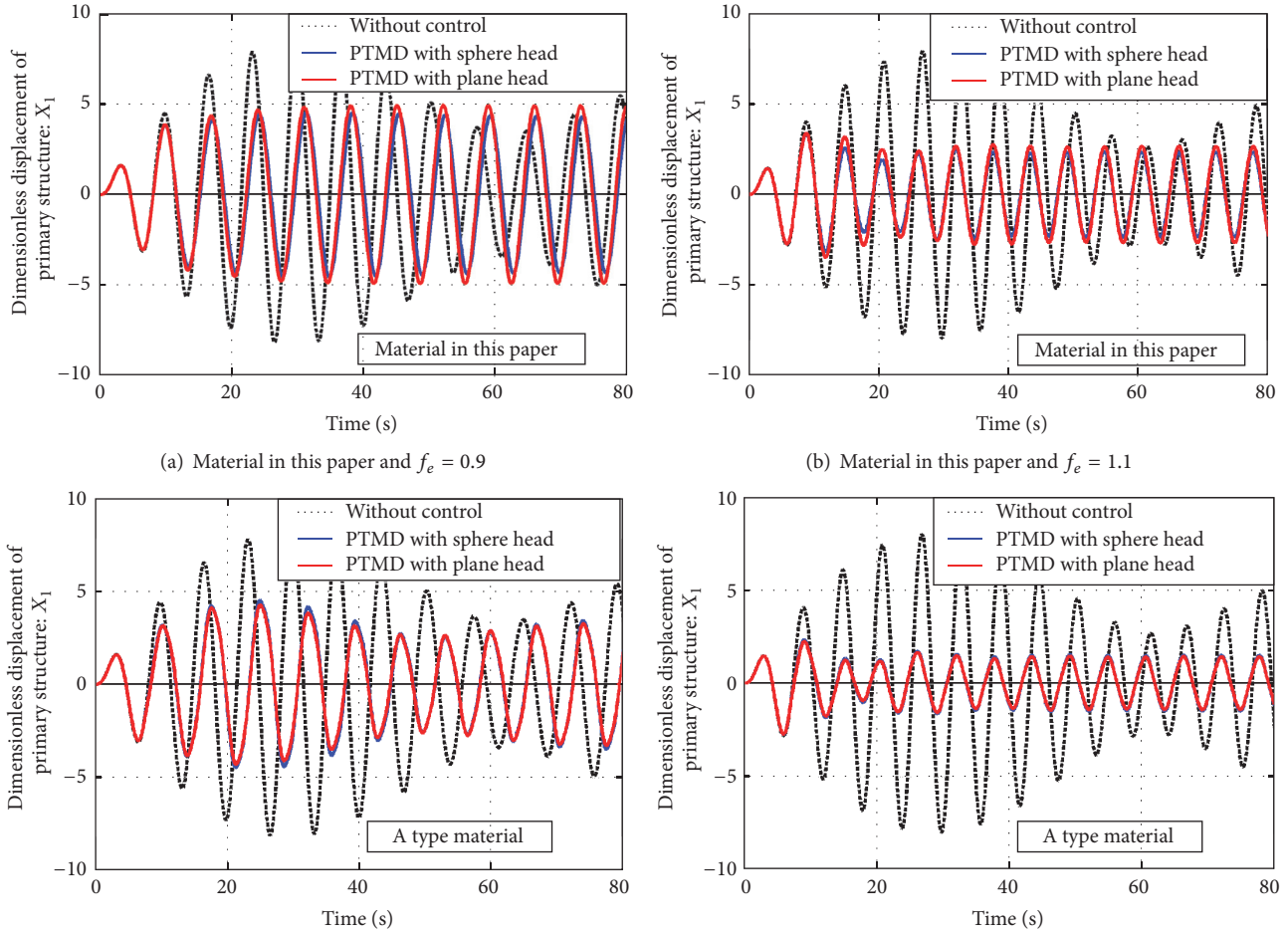

(a) Material in this paper and $f_e = 0.9$ (b) Material in this paper and $f_e = 1.1$

(c) A type material and $f_e = 0.9$ (d) A type material and $f_e = 1.1$

Figure 8: Control performance of PTMD with different contact geometries.

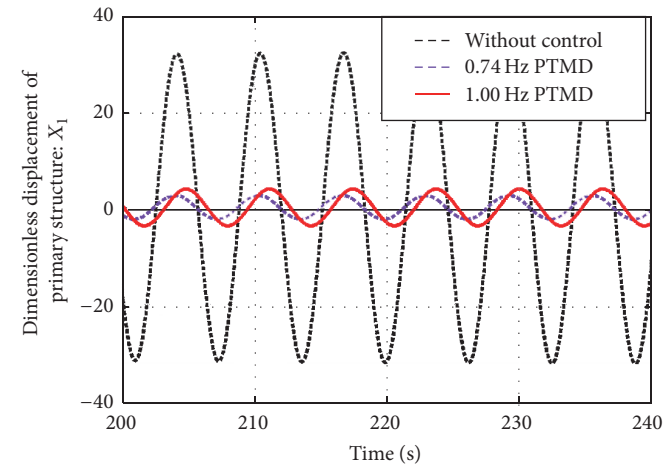

(a) Controlled by PTMD

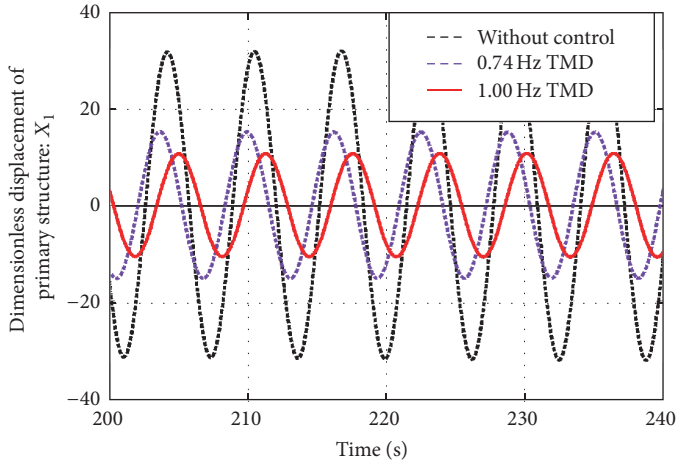

(b) Controlled by TMD

Figure 9: Control performance of TMD and PTMD in tuned excitation vibration.

As a comparison, the control performance of the TMD with the same detuning ratio is plotted in Figure 10(b). It will take 63.7 s and 61.3 s to reduce the maximum displacement to 8 mm for 0.74 Hz and 1.00 Hz, respectively. This is nearly three times as much as PTMD under 0.74 Hz and four times of a 1.00 Hz TMD. The simulation result demonstrates that PTMD can suppress the vibration and dissipate energy more effectively and show excellent adaptability and strong robustness.

5.3. Detuning Excitation Vibration. To evaluate the control performance of PTMD under free vibration excitation, four vibration reduction ratios named $\eta_{A1,\text{peak,PTMD}}$, $\eta_{\text{RMS}A1,\text{PTMD}}$, $\eta_{X1,\text{peak,PTMD}}$, and $\eta_{\text{RMS}X1,\text{PTMD}}$ are defined as (16). For TMD, $\eta_{A1,\text{peak,TMD}}$, $\eta_{\text{RMS}A1,\text{TMD}}$, $\eta_{X1,\text{peak,TMD}}$, and $\eta_{\text{RMS}X1,\text{TMD}}$ have similar definitions:

$$\eta_{A1,\text{peak,PTMD}} = \frac{A_{1,\text{peak,NO}} - A_{1,\text{peak,PTMD}}}{A_{1,\text{peak,NO}}} \times 100\%$$

$$\eta_{X1,\text{peak,PTMD}} = \frac{X_{1,\text{peak,NO}} - X_{1,\text{peak,PTMD}}}{X_{1,\text{peak,NO}}} \times 100\%$$

$$\eta_{\text{RMS}A1,\text{PTMD}} = \frac{\text{RMS}_{A_1,\text{NO}} - \text{RMS}_{A_1,\text{NO}}}{\text{RMS}_{A_1,\text{NO}}} \times 100\%$$

$$\eta_{\text{RMS}X1,\text{PTMD}} = \frac{\text{RMS}_{X_1,\text{NO}} - \text{RMS}_{X_1,\text{NO}}}{\text{RMS}_{X_1,\text{NO}}} \times 100\%. \quad (16)$$

Figure 11 illustrates the relationship between reduction of peak value and DTR when the primary structure is applied by a series of detuning sinusoidal waves. From Figures 11(a) to 11(d), we can see that the performance will stay in a desired level and is barely affected by the DTR in case of being subjected to uptuned sinusoidal wave excitation ($f_e \geq 1$).

In Figure 11(a), PTMD shows an excellent performance with reduction of about 82.5% in case of $f_e = 1$ and only has tiny deterioration with DTR increasing. For $f_e = 1.1$ and $f_e = 1.2$, the reductions are almost kept as constants with reduction values of 50.5% and 33.8%, respectively. For downtuned cases ($f_e < 1$), the values of DTR have significant influences on reductions. In case of $f_e = 0.9$, reduction decreases sharply from 58.7% to 2.3% with DTR changing

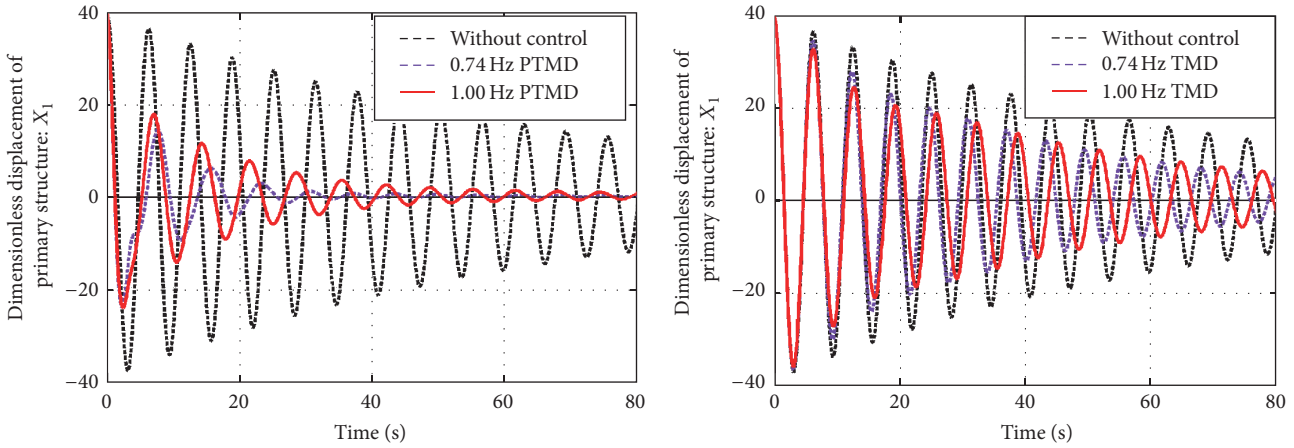

(a) Controlled by PTMD (b) Controlled by TMD

Figure 10: Control performance of PTMD and TMD in free vibration excitation.

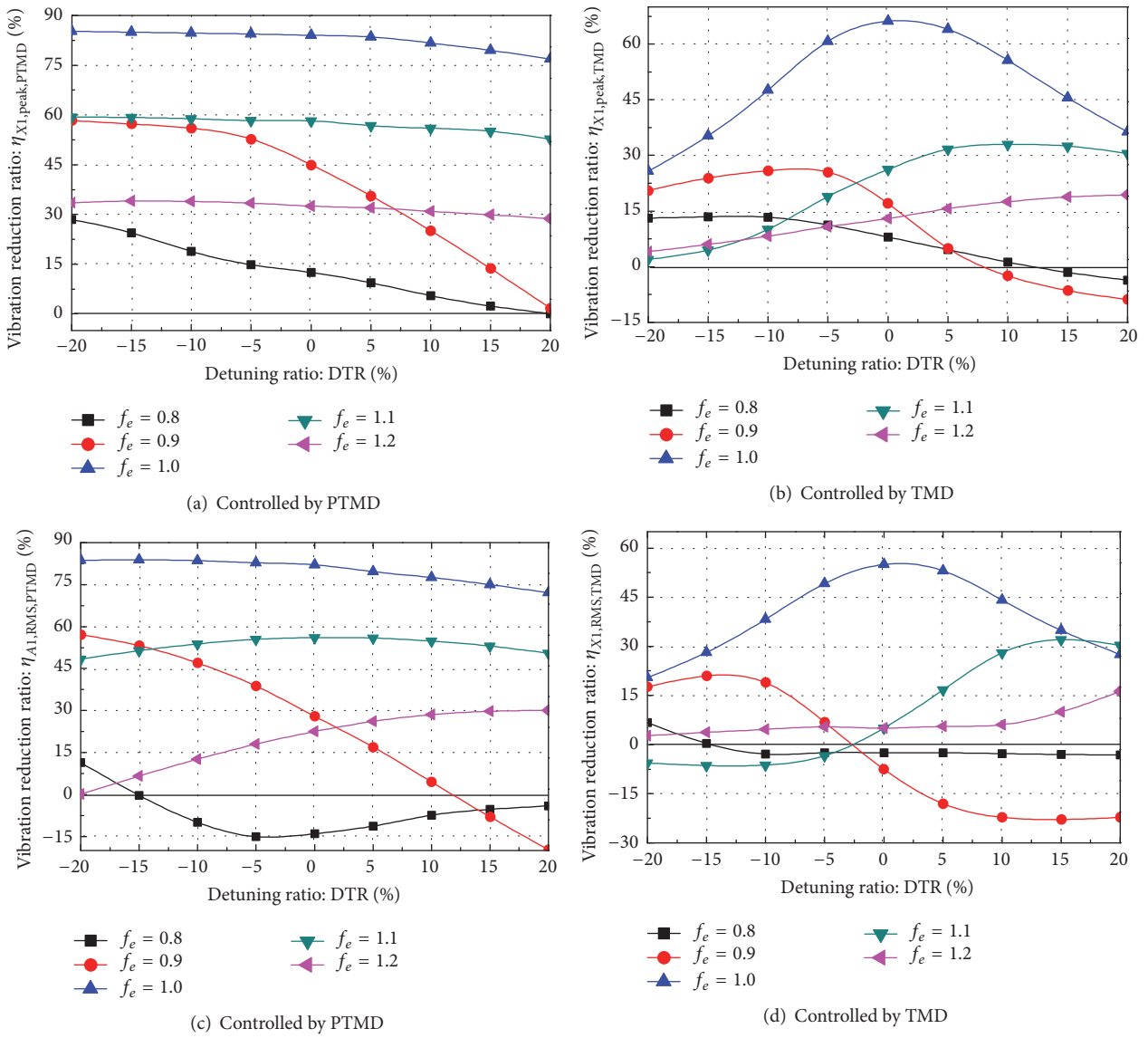

(a) Controlled by PTMD (b) Controlled by TMD

(c) Controlled by PTMD (d) Controlled by TMD

Figure 11: Control performance of TMD and PTMD in detuning excitation vibration.

from −20% to 20%. In case of $f_e = 0.8$, it will decline from 28.9% to 0 nearly in a linear relationship.

From Figure 11(c), vibration reduction of PTMD on RMS of displacement changes from 72.8% to 82.0% in case of $f_e = 1.0$ and varies between 48.4% and 56.1% when f_e is equal to 1.1. This is almost the same as the maximum reduction value in Figure 11(a). However, PTMD shows a relatively poor performance with the value of f_e equal to 1.2. Although the reduction is 30.2%, PTMD rarely works when DTR is −20% in that situation. In addition, reduction decreases sharply from 57.2% to −19.7% when f_e is equal to 0.9, which has a similar tendency in Figure 11(a). In case of $f_e = 0.8$, reduction is minus as DTR varies from −15% to 20%. This means that PTMD has an adverse effect on vibration control performance.

Figures 11(b) and 11(d) display control performance of TMD. It can be seen that TMD is effective when the structure is subjected to tuned excitation ($f_e = 1.0$) especially when the TMD is tuned (DTR = 0). However, TMD's performance is not as stable as PTMD subjected to tuned excitation. For instance, the value of $\eta_{X1,\text{peak,TMD}}$ is 66.2% for tuned TMD, but only 25.8% for a downtuned TMD (corresponding to DTR = −20%).

As an improvement of TMD, PTMD's seismic vibration reduction mechanism mainly includes two parts: on the one hand, controlling force comes from the relative motion between mass block and primary structure, which is the most important reduction mechanism of a traditional TMD. On the other hand, pounding force induced by impact can be regarded as an extra controlling force just as an impact damper, in which energy can be dissipated during the impact between mass block and viscoelastic material. When a tuned wave ($f_e = 1$) is input into the system and a sufficient relative motion can be achieved, both PTMD and TMD show satisfactory reduction results.

However, reduction of TMD decreases due to dramatic falling in relative motion when the controlled platform is under detuning excitation ($f_e \neq 1$). As evidence shown in Figure 11(c), $\eta_{X1,\text{peak,TMD}}$ decreases from 66.22% to 26.2% as f_e changes from 1 to 1.1. Unlike TMD, PTMD shows a superior performance even when the structure is subjected to a detuning wave. This is because controlling force from impact is considerable and high energy dissipation happens during the impact process even when the relative motion is very small. As a comparison result in Figure 11(a), the value of $\eta_{X1,\text{peak,PTMD}}$ for a tuned PTMD declines from 84.3% to 58.3% when f_e changes from 1 to 1.1. For a lager detuning ratio of seismic effect ($f_e = 1.2$), $\eta_{X1,\text{peak,PTMD}}$ turns to 32.5% compared to 13.4% for TMD.

6. Comparisons between PTMD and TMD with Optimal Parameters

6.1. Vibration Reduction. The variations of reduction responses for PTMD and TMD which are subjected to different frequency sinusoidal waves are plotted in Figure 12.

In terms of acceleration (Figures 12(a) and 12(b)), the traditional TMD can significantly reduce both of the peak value and the RMS when the seismic frequency is tuned to the natural frequency ($f_e = 1$), which can be up to 71.7% and 63.1%, respectively. However, higher reduction ratios of 85.8% and 80.6% can be achieved by the PTMD, which shows a better control performance than TMD. When the seismic effect deviates from the natural frequency of primary structure ($f_e \neq 1$), more excellent effects can also be obtained for PTMD by an average of 14% higher than TMD on peak acceleration reduction (Figure 12(a)).

For RMS of acceleration, vibration reduction of TMD ratios is minus when f_e varies from 0.78 to 0.91 and from 1.09 to 1.16 (Figure 12(b)). This means that the TMD magnifies the vibration responses of the offshore jacket platform, and, at this time, TMD is not recommended in the primary structure. In contrast, PTMD maintains an excellent performance within all the range of frequency ratios.

In terms of displacement (Figures 12(c) and 12(d)), more superior reductions are also achieved by the PTMD. The peak value and RMS of dimensionless displacement can be reduced by 86.6% and 84.5% when $f_e = 1$. This reduction is higher than TMD, whose corresponding reductions are 71.5% and 64.9%. Moreover, more effective performance has been observed with the PTMD in most cases except for f_e that ranges from 0.7 to 0.8 for RMS. The analysis results illustrate the fact that, in almost all cases, PTMD is far more effective than TMD on vibration control performance.

6.2. Effective Frequency Bandwidth. To achieve the best vibration control effect, the frequency of sinusoidal wave must be limited to a certain scope when the structure is equipped with TMD. In general, vibration control technique often fails when the frequency of applied load deviates from the structure frequency by more than 10%. Given the randomness of earthquake wave, this technique has its own limitations unavoidably. To quantify the effective bandwidth of TMD and PTMD, l_e is defined as in the following equation:

$$l_e = \left| f_{e1}(\eta_0) - f_{e2}(\eta_0) \right|, \tag{17}$$

where η_0 is the required control vibration reduction ratio and $f_{e1}(\eta_0)$ and $f_{e2}(\eta_0)$ are two responding frequencies. l_e measures the range of frequencies in which TMD or PTMD can meet the given requirements. And the larger the value of l_e is, the wider the effective frequency bandwidth is. In other words, a control device with a wider bandwidth is much more adaptive in seismic control.

Figures 13 and 14 illustrate the comparison of effective bandwidths between PTMD and TMD under a given requirement. It is clear that PTMD shows a wider bandwidth on acceleration (Figure 13) and displacement (Figure 14) than TMD for the same required control vibration reduction ratio. Furthermore, it can be observed from Figure 14 that effective bandwidth of PTMD expands approximately twice as much as TMD on RMS displacement.

For peak value of displacement shown in Figure 14(a), PTMD still has distinct advantages. When the reduction requirement is 10%, peak values of displacement are 0.67 for PTMD and 0.47 for TMD. This difference is the closest gap

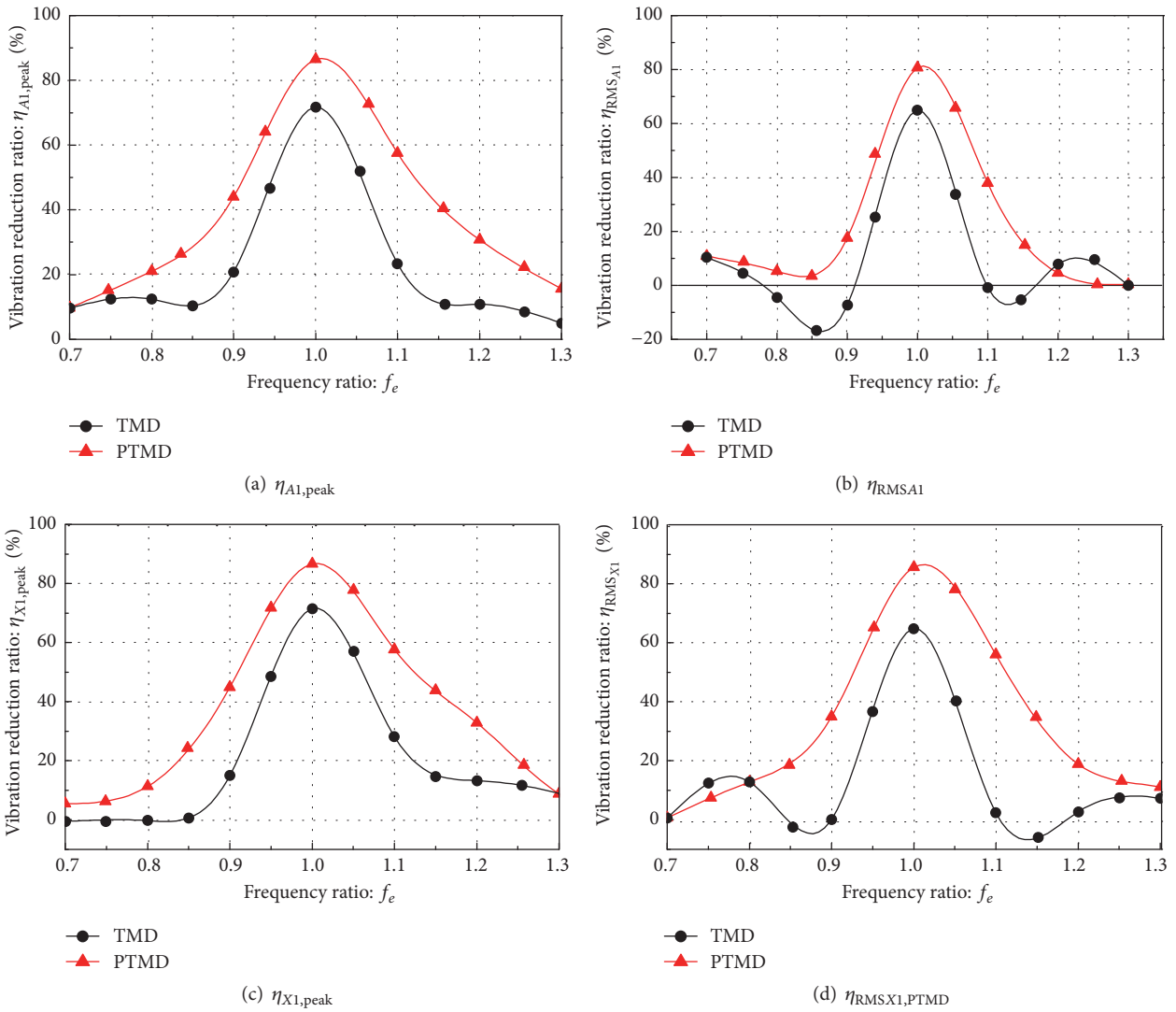

FIGURE 12: The comparison of η between PTMD and TMD with optimal parameter (PTMD: $\xi_2 = 3\xi_{opt}$, $\delta = 2$, and $\mu = 2\%$; TMD: $\xi_2 = 3\xi_{opt}$, $\mu = 2\%$).

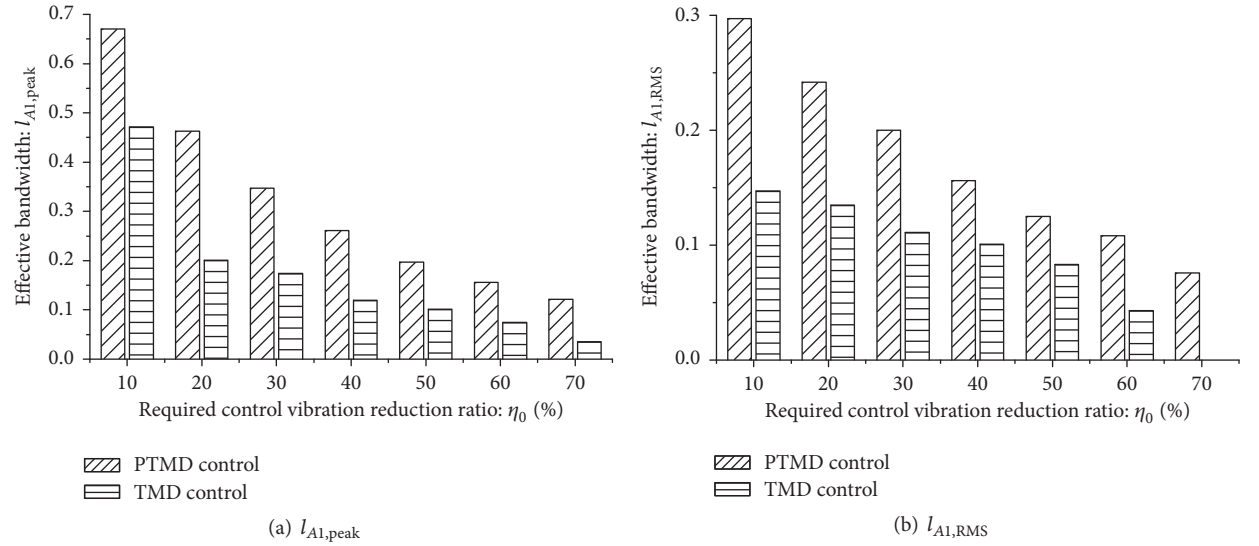

FIGURE 13: Comparison of effective bandwidth on dimensionless acceleration.

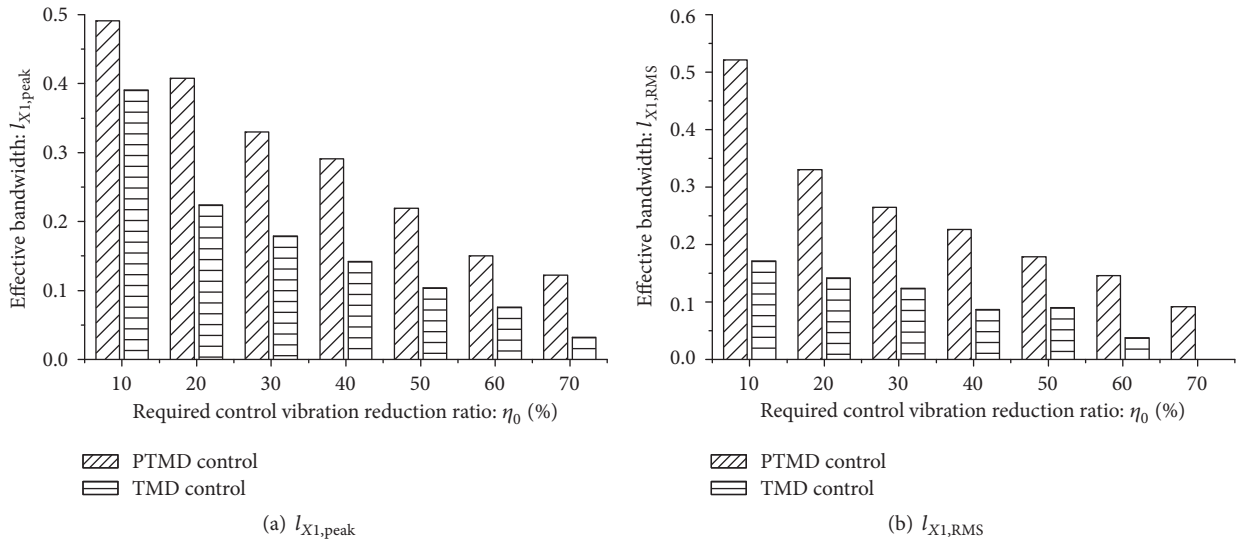

FIGURE 14: Comparison of effective bandwidth on dimensionless displacement.

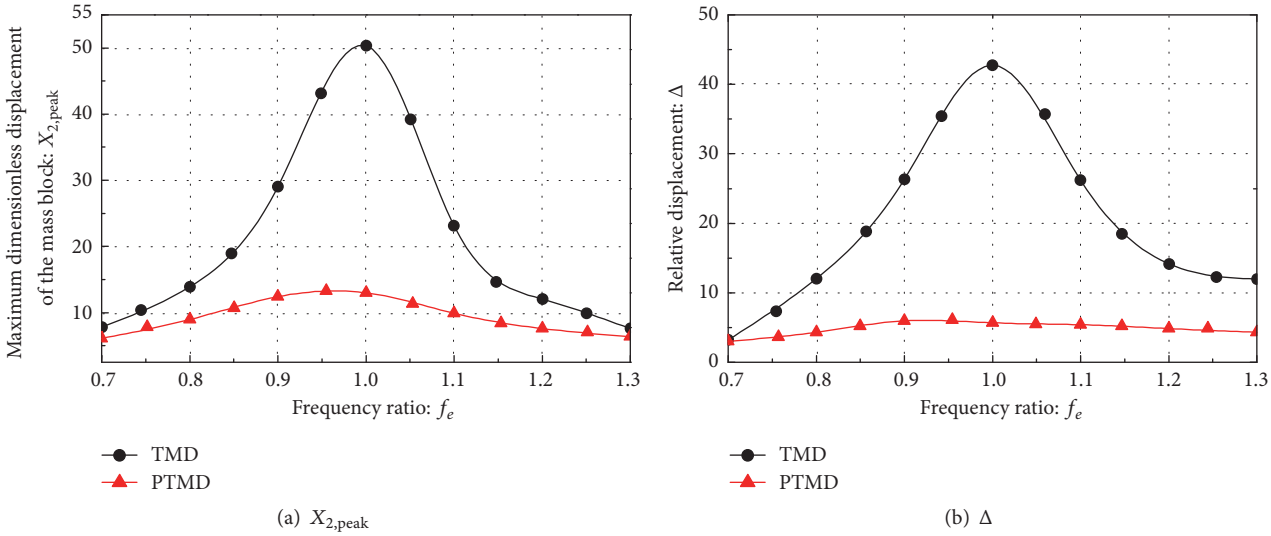

FIGURE 15: Response of the mass block and relative displacement (PTMD: $\xi_2 = 3\xi_{opt}$, $\delta = 2$, and $\mu = 2\%$; TMD: $\xi_2 = 3\xi_{opt}$, $\mu = 2\%$).

between the devices among others. Otherwise, PTMD makes nearly double the reduction that TMD does.

In terms of acceleration, PTMD has superior performance over the traditional TMD both in peak value (Figure 14(a)) and in the RMS (Figure 14(b)). When the goal for peak value of displacement is 70%, the bandwidth is only 0.032, which means TMD only allows the seismic effect to deviate by 1.6% from the tuned sinusoidal wave since the reduction is almost center symmetry by $f_e = 1$ (Figure 12). In other words, the device is almost useless since it is practically impossible for the structure subjected to a tuned seismic effect. But for PTMD, the bandwidth is 0.122. Even for a lower requirement, like 30%, values of $l_{A1,peak}$ are 0.347 and 0.174 for PTMD and TMD, respectively. In terms of $l_{X1,peak}$, they are 0.330 and 0.179 for PTMD and TMD, respectively. The bandwidth results indicate that PTMD can be applied to different earthquake patterns.

6.3. Costs and Installing Space. A superpower continuous working damper needs to be equipped for TMD due to the large mass of block and continuous movement. Except for high cost, a huge space for installing is a primary need to achieve satisfying control effects.

Figure 15(a) presents the peak value of the dimensionless displacement of the mass block under different excitations. The maximum of the value for TMD can be as large as 50.3 while it is only 12.4 for PTMD. The value of TMD decreases rapidly, but it is smaller in the frequency domain for PTMD. Therefore, the movement of the mass block is significantly reduced due to the limiter, and this means that the cost of additional dampers can be drastically discarded.

The relative displacement is defined as Δ in the following equation:

$$\Delta = \left|X_1 - X_2\right|_{\max}, \tag{18}$$

where X_1 and X_2 are dimensionless displacement values for primary structure and mass block, respectively. Δ represents the minimum space requirement for installing. Figure 15(b) illustrates the relationship between Δ of different controlling techniques. It can be observed that at least the minimum value of dimensionless space is 42.8 which must be provided to TMD for motion. But for PTMD, the value is 5.9, which is only 13.7% of TMD.

7. Conclusion

A SDOF structure simplified from JZ20-2MUQ type offshore jacket platform is taken as an example to investigate the seismic control performance and robustness of PTMD. The following conclusions can be obtained:

(1) Damping ratio is extremely important for PTMD. Although an additional damper will enhance the efficiency of PTMD, an exceeding damping ratio may have the opposite effect. And the optimal damping ratio which is based on TMD is no longer applicable for PTMD due to the impact effect. The optimal damping ratio value for PTMD is about three times that of the TMD in this paper.

(2) The gap between the mass block and the viscoelastic layer is another key factor for vibration reduction. Since impact may have adverse influences on the control performance when the platform is subjected to low frequency excitation, an appropriate gap should be reserved.

(3) Control performance of PTMD is sensitive to properties of material. A material with higher equivalent elasticity modulus can enhance the efficiency when the excitation frequency is higher than the natural frequency of primary structure. Otherwise, it will weaken the vibration reduction. But contact geometries have little effect on PTMD's vibration reduction.

(4) Tuned excitation vibration, detuning vibration, and free vibration are present to investigate the robustness of PTMD. The simulation results show more excellent vibration mitigation in all cases compared to TMD. Comparison between PTMD and traditional TMD verifies the advantages of PTMD not only in vibration suppression and costs, but also in effective frequency bandwidth.

Competing Interests

The authors declare that there are no competing interests regarding the publication of this paper.

Acknowledgments

The research is supported by the National Natural Science Foundation of China (Projects nos. 51678322 and 51409056), the Natural Science Foundation of Heilongjiang Province (E2015047, E2015045), the Fundamental Research Funds for the Central Universities (HEUCF160202), and the Taishan Scholar Priority Discipline Talent Group program funded by Shandong Province.

References

[1] S. Chandrasekaran, A. K. Jain, and N. R. Chandak, "Seismic analysis of offshore triangular tension leg platforms," *International Journal of Structural Stability and Dynamics*, vol. 6, no. 1, pp. 97–120, 2006.

[2] A. Ajamy, M. R. Zolfaghari, B. Asgarian, and C. E. Ventura, "Probabilistic seismic analysis of offshore platforms incorporating uncertainty in soil-pile-structure interactions," *Journal of Constructional Steel Research*, vol. 101, pp. 265–279, 2014.

[3] K. Kawano, K. Furukawa, and K. Venkataramana, "Seismic response of offshore platform with TMD," in *Proceedings of the 10th World Conference on Earthquake Engineering*, pp. 2241–2246, Balkema, Rotterdam, 1992.

[4] Q. Wu, X. Zhao, R. Zheng, and K. Minagawa, "High response performance of a tuned-mass damper for vibration suppression of offshore platform under earthquake loads," *Shock and Vibration*, vol. 2016, Article ID 7383679, 11 pages, 2016.

[5] J. L. Almazan, J. C. De la Llera, J. A. Inaudi, D. Lopez-Garcia, and L. E. Izquierdo, "A bidirectional and homogeneous tuned mass damper: a new device for passive control of vibrations," *Engineering Structures*, vol. 29, no. 7, pp. 1548–1560, 2007.

[6] M.-H. Chey, J. G. Chase, J. B. Mander, and A. J. Carr, "Semi-active tuned mass damper building systems: design," *Earthquake Engineering and Structural Dynamics*, vol. 39, no. 2, pp. 119–139, 2010.

[7] C. Sun and S. Nagarajaiah, "Study on semi-active tuned mass damper with variable damping and stiffness under seismic excitations," *Structural Control and Health Monitoring*, vol. 21, no. 6, pp. 890–906, 2014.

[8] A. Jafarabad, M. Kashani, M. R. A. Parvar, and A. A. Golafshani, "Hybrid damping systems in offshore jacket platforms with float-over deck," *Journal of Constructional Steel Research*, vol. 98, pp. 178–187, 2014.

[9] M. Mohebbi, H. Rasouli, and S. Moradpour, "Assessment of the design criteria effect on performance of multiple tuned mass dampers," *Advances in Structural Engineering*, vol. 18, no. 8, pp. 1141–1158, 2015.

[10] L.-S. Huo and H.-N. Li, "Torsionally coupled response control of offshore platform structures using circular tuned liquid column dampers," *China Ocean Engineering*, vol. 18, no. 2, pp. 173–183, 2004.

[11] H.-N. Li, X.-Y. He, and L.-S. Huo, "Seismic response control of offshore platform structures with shape memory alloy dampers," *China Ocean Engineering*, vol. 19, no. 2, pp. 185–194, 2005.

[12] J. Ou, X. Long, Q. S. Li, and Y. Q. Xiao, "Vibration control of steel jacket offshore platform structures with damping isolation systems," *Engineering Structures*, vol. 29, no. 7, pp. 1525–1538, 2007.

[13] Y. Komachi, M. R. Tabeshpour, A. A. Golafshani, and I. Mualla, "Retrofit of Ressalat jacket platform (Persian Gulf) using friction damper device," *Journal of Zhejiang University: Science A*, vol. 12, no. 9, pp. 680–691, 2011.

[14] S. A. Mousavi, S. M. Zahrai, and K. Bargi, "Optimum geometry of tuned liquid column-gas damper for control of offshore jacket platform vibrations under seismic excitation," *Earthquake Engineering and Engineering Vibration*, vol. 11, no. 4, pp. 579–592, 2012.

[15] S. A. Mousavi, K. Bargi, and S. M. Zahrai, "Optimum parameters of tuned liquid columngas damper for mitigation of seismic-induced vibrations of offshore jacket platforms," *Structural Control and Health Monitoring*, vol. 20, no. 3, pp. 422–444, 2013.

[16] A. Sarrafan, S. H. Zareh, A. A. A. Khayyat, and A. Zabihollah, "Neuro-fuzzy control strategy for an offshore steel jacket platform subjected to wave-induced forces using magnetorheological dampers," *Journal of Mechanical Science and Technology*, vol. 26, no. 4, pp. 1179–1196, 2012.

[17] M. A. Lotfollahi-Yaghin, H. Ahmadi, and H. Tafakhor, "Seismic responses of an offshore jacket-type platform incorporated with tuned liquid dampers," *Advances in Structural Engineering*, vol. 19, no. 2, pp. 227–238, 2016.

[18] P. Zhang, G. Song, H.-N. Li, and Y.-X. Lin, "Seismic control of power transmission tower using pounding TMD," *Journal of Engineering Mechanics*, vol. 139, no. 10, pp. 1395–1406, 2013.

[19] H. Li, P. Zhang, G. Song, D. Patil, and Y. Mo, "Robustness study of the pounding tuned mass damper for vibration control of subsea jumpers," *Smart Materials and Structures*, vol. 24, no. 9, pp. 135–142, 2015.

[20] L. Li, G. Song, M. Singla, and Y.-L. Mo, "Vibration control of a traffic signal pole using a pounding tuned mass damper with viscoelastic materials (II): experimental verification," *JVC/Journal of Vibration and Control*, vol. 21, no. 4, pp. 670–675, 2015.

[21] G. Song, P. Zhang, L. Li et al., "Vibration control of a pipeline structure using pounding tuned mass damper," *Journal of Engineering Mechanics*, vol. 142, no. 6, Article ID 04016031, 2016.

[22] P. Zhang, L. Li, D. Patil et al., "Parametric study of pounding tuned mass damper for subsea jumpers," *Smart Materials & Structures*, vol. 25, no. 1, Article ID 015028, 2016.

[23] J. P. Ou, X. Long, Y. Q. Xiao, and B. Wu, "Damping isolation system and its vibration-suppressed effectiveness analysis for offshore platform jacket structures," *Earthquake Engineering and Engineering Vibration*, vol. 6, no. 1, pp. 115–122, 2002.

[24] Q. Xue, C. Zhang, J. He, G. Zou, and J. Zhang, "An updated analytical structural pounding force model based on viscoelasticity of materials," *Shock and Vibration*, vol. 2016, Article ID 2596923, 15 pages, 2016.

[25] T. Ioi and K. Ikeda, "On the houde damper for a damped vibration system," *Bulletin of the JSME*, vol. 23, no. 176, pp. 273–279, 1980.